RSC Advances

PAPER

View Article Online
View Journal | View Issue

A ternary Er^{3+}-$BiVO_4/TiO_2$ complex heterostructure with excellent photocatalytic performance

Cite this: *RSC Adv.*, 2014, **4**, 6920

S. Obregón and G. Colón*

Received 12th November 2013
Accepted 23rd December 2013

DOI: 10.1039/c3ra46603e

www.rsc.org/advances

Ternary erbium doped $BiVO_4/TiO_2$ complexes are synthesized by means of a simple impregnation method with good photoactivities under sun-like excitation for the degradation of phenol. From the structural and morphological characterization it has been stated that the presence of Er^{3+} induces a slight stabilization of the tetragonal phase probably due to its incorporation in the $BiVO_4$ lattice. Therefore a ternary heterostructured material has been obtained. The best photocatalytic performance was attained for the samples with 1 wt% of Er^{3+}-doped $BiVO_4$ content with respect to TiO_2. The occurrence of a complex structural mixture with the adequate band position leads to effective charge pair separation which induces higher photocatalytic activities.

1. Introduction

Visible-light-induced semiconductor photocatalysts have revealed great potential applications in elimination of organic pollutants.[1] However, most of the proposed semiconductor photocatalysts are clearly restricted by their poor efficiency. Within this framework, bismuth vanadate (*m*-$BiVO_4$) has been proposed as a novel alternative for TiO_2-based photocatalysis. Thus, in the last few years, many studies described the interesting performances of $BiVO_4$ for organic contaminants degradation as well as O_2 evolution reactions under visible-light irradiation.[2–6]

It has been widely reported that the photocatalytic performance of $BiVO_4$ is strongly dependent on its morphology and microstructure.[7–10] Different synthetic routes leads to $BiVO_4$ in two crystalline phases: monoclinic (space group *I*2/*b*) and tetragonal (space group $I4_1/a$) scheelite.[11,12] Among the above crystal phases, the monoclinic $BiVO_4$ is the best visible-light-driven photocatalyst. The results reported by Yu *et al.* demonstrated that the crystalline structure is the vital factor controlling *MB* degradation and O_2 evolution reactions.[13] In the same direction, Tokunaga *et al.* reported that monoclinic structure shows much higher activity than a tetragonal one for O_2 evolution reaction.[14] From DFT calculations it is proposed that the effective hybridization of Bi6s state and the O2p state at the top of the valence band would be the responsible of the lower band gap value exhibited by *m*-$BiVO_4$ (*ca.* 2.4 eV) (Scheme 1).[15,16]

On the basis of the wide reported results, the photocatalytic activity of tetragonal $BiVO_4$ appears almost negligible[17–19] while the photocatalytic activity of *m*-$BiVO_4$ is still scarce due to the poor charge-transport characteristics and the weak surface adsorption properties of this material.[20,21] Therefore, it is necessary to develop effective strategies to improve the charge separation efficiency and enhance visible-light photocatalytic activity of $BiVO_4$ photocatalysts.

For the photoactivity improvement sake, different approaches have been proposed which include heterojunction structure formation,[20,22,23] co-catalysts loading,[24,25] and impurity doping.[26,27] Among these approaches, the co-existence of monoclinic-tetragonal heterostructure appears as a new way to be considered. Recently, it has been stated that the existence of a mixed-phase $BiVO_4$ clearly show higher photocatalytic activity.[28] The improved photocatalytic performance of *m*–*t* heterostructured $BiVO_4$ has been associated to promotion photoinduced electron–hole pairs separation.[29] Within this framework, Obregón *et al.* reported the unexpected enhanced photocatalytic activity of tetragonal stabilized Ln-doped $BiVO_4$.[30,31] Moreover, by changing the precursor addition sequence in the synthesis route, we have obtained a monoclinic-

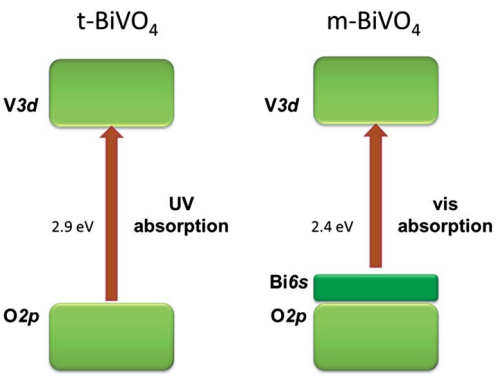

Scheme 1 Schematic band structures of the *t*-$BiVO_4$ and *m*-$BiVO_4$.

Instituto de Ciencia de Materiales de Sevilla, Centro Mixto CSIC-Universidad de Sevilla, C/Américo Vespucio, 49, 41092 Sevilla, Spain. E-mail: gcolon@icmse.csic.es; Tel: +34 954489536

tetragonal heterostructured Er^{3+}-$BiVO_4$ exhibiting notably a high photoactivity under sun-like irradiation.[32] For this system, we have stated that the presence of erbium provokes a significantly higher photoactivity that could be related to a double complex mechanism. Firstly, the formation of the tight interface *m–t* heterostructure could be the responsible of a more effective charge separation. And secondly, but not less important, the contribution of extra-photons generated by a cooperative luminescence process in the overall mechanism due an energy transfer process from erbium ions to *t*-$BiVO_4$ and *m*-$BiVO_4$ could enhance the photon efficiency of the photocatalytic process.

Thus, as the formation of heterojunction can significantly reduce the recombination and speed up the separation rate of photogenerated charge carriers, coupling $BiVO_4$ with other semiconductors are often used as an effective modification method. Within this frame, Long *et al.* proposed the Co_3O_4/$BiVO_4$ composite photocatalyst ash a p–n heterojunction semiconductor. These authors showed that the composite photocatalyst presented much higher photoactivity than pure $BiVO_4$ in the degradation of phenol under visible light irradiation.[33] Moreover, other authors reported a V_2O_5/$BiVO_4$ composite exhibiting the enhanced photocatalytic performance.[34,35] Finally, the photocatalytic properties of coupled TiO_2/$BiVO_4$ have been also recently investigated demonstrating the interest of $BiVO_4$ based heterojunctions.[36,37] However, in these later cases *m*-$BiVO_4$ has been considered. Taking into account *m*-$BiVO_4$ conduction and valence bands position with respect to TiO_2, it is clear that an unfavourable situation is taking place. In the present paper we present a ternary complex heterostructure formed by TiO_2 anatase and monoclinic-tetragonal $BiVO_4$ by erbium doping. The photocatalytic activities were evaluated by the photodegradation of phenol under simulated sun-light irradiation and the possible electronic mechanism responsible of the enhanced photocatalytic activities of Er^{3+}-doped $BiVO_4$/TiO_2 composite photocatalysts was also discussed.

2. Experimental

2.1 Samples preparation

TiO_2 sample was obtained by means of a hydrothermal method elsewhere described.[38] In brief, a TiO_2 colloidal solution was obtained by adding certain amount of Ti^{4+}–isopropanol solution to 400 mL of distilled water at pH = 2 achieved by means of acetic acid. After TTiP addition a white precipitate is obtained that upon stirring at room temperature for one week evolve to a milky homogeneous solution. A certain amount of triethylamine (TEA) was then added drop wise to the Ti-solution aliquot till the pH value was 9. Afterwards, the obtained white precipitate suspension was then placed in a Teflon recipient inside of stainless steel autoclave reactor. The hydrothermal treatment was performed at 120 °C, 20 hours. The as obtained precipitate was then filtered, repeatedly washed and dried overnight at 120 °C. Then TiO_2 powder was submitted to a further calcination treatment at 300 °C for 2 hours.

On the other hand, for the preparation of Er^{3+} doped $BiVO_4$, we have followed the method previously reported.[32] Briefly, 5 mmol of $Bi(NO_3)_3 \cdot 5H_2O$ was dissolved in 10 mL of glacial acetic acid at room temperature. A second aqueous solution was prepared by dissolving the corresponding stoichiometric amount of NH_4VO_3 and the corresponding amount of $Er(NO_3)_3$ (0.75 at.%) in 60 mL of hot distilled water. A milky colloidal suspension is obtained which could indicate the formation of small $ErVO_4$ particles. Afterwards, the ammonium metavanadate solution was added to the bismuth nitrate aqueous solution and the process was accompanied with a vigorous stirring. The pH of the obtained suspension was adjusted to 9.0 by adding concentrated NH_4OH (13 mol L^{-1}). The slurry was encased in a Teflon vessel and heated under microwave irradiation using a microwave reactor. The temperature was fixed at 140 °C with a maximum variable power of 195 W during 30 min. The obtained precipitate was then cooled until room temperature, filtered and repeatedly washed and dried overnight at 120 °C. Afterwards, thus obtained samples were submitted to a further calcination treatment at 300 °C for 2 h.

Hybrid composites were achieved by simple impregnation method previously described.[39] In a typical procedure, the appropriate amounts of TiO_2 and Er-$BiVO_4$ were added into methanol and sonicated separately for 30 min. Then, these two solutions were mixed and stirred at room temperature for 24 h. Afterwards, the composite photocatalysts were obtained by evaporating the methanol at 80 °C. Er-$BiVO_4$ contents ranged from 0.5 wt% to 5 wt% with respect to TiO_2.

2.2 Materials characterization

BET surface area and porosity measurements were carried out by N_2 adsorption at 77 K using a Micromeritics 2010 instrument.

X-ray diffraction (XRD) patterns were obtained using a Siemens D-501 diffractometer with Ni filter and graphite monochromator. The X-ray source was Cu Kα radiation (0.15406 nm). The diffraction patterns were recorded from 2θ 10° to 80° with step of 0.05° and 120 s per step. Crystallite sizes were obtained from Rietveld refinement.

The UV diffuse reflectance spectra were measured using an UV-vis spectrophotometer equipped with an integrating sphere (JASCO V-570). The reference sample used was a $BaSO_4$ coated standard pattern.

Micro-Raman measurements were performed using a Lab-RAM Jobin Yvon spectrometer equipped with a microscope. Laser radiation (λ = 532 nm) was used as excitation source at 5 mW. All measurements were recorded under the same conditions (2 s of integration time and 30 accumulations) using a 100× magnification objective and a 125 mm pinhole.

Field emission scanning electron (FE-SEM) and Transmission electron microscopy (TEM) was performed by using a Hitachi S 4800 and Philips CM 200 microscopes, respectively. The samples were dispersed in ethanol using an ultrasonicator and dropped on a carbon grid.

2.3 Photocatalytic tests

The photocatalytic activity of the samples was tested by means the degradation of phenol under simulated solar conditions. In

a typical procedure, 0.05 g of photocatalyst was placed in a batch reactor containing 50 mL of phenol whose initial concentration was 30 mg L^{-1}. The suspension was maintained under dark conditions for 15 min in order to achieve the adsorption–desorption equilibrium of the dye on the photocatalyst surface. Afterwards, the suspension was irradiated with simulated solar light by means a solar simulator PEC-L01, Peccell. Samples of 1 mL were taken at given interval times and the photocatalyst was separated using a nylon filter. The concentrations were monitored by checking the absorption spectrum of each sample through its absorption band maximum (270 nm) using an UV-vis spectrophotometer (MECASYS Optizen 2120UV).

3. Results and discussion

We have prepared a simple heterostructure based on TiO_2 and Er-$BiVO_4$ systems. The structural characterization of both was already reported by us.[32,38] The sol–gel hydrothermal preparation of TiO_2 from colloidal suspension leads to anatase phase system with calculated crystallite size of *ca.* 15 nm (Table 1). On the other hand, it has been stated that the incorporation of Er^{3+} in the $BiVO_4$ structure induces the stabilization of the tetragonal structure (Fig. 1).

Such structural stabilization has been explaining by considering the formation of small $ErVO_4$ seeds during the synthetic procedure, previous to the $BiVO_4$ formation.[32] $ErVO_4$ is normally obtained in the tetragonal zircon structure.[40] These small seeds would act as structure-directing agent conditioning the formation of the tetragonal $BiVO_4$. Thus, a mixture of monoclinic and tetragonal phase is obtained, being the tetragonal the predominant one (70% tetragonal *vs.* 30% monoclinic). The XRD patterns of composite systems denote the presence of former structures, anatase TiO_2 and the corresponding growing fraction of tetragonal-monoclinic mixture of Er-$BiVO_4$ (Fig. 1).

The BET surface area of TiO_2 is found to be significantly high, *ca.* 102 m^2 g^{-1}. On the contrary and as widely reported in the literature, for $BiVO_4$ the surface area values are considerably low, always below 1–2 m^2 g^{-1} (Table 1).[41,42] The occurrence of the tetragonal phase clearly induces a certain increase in this feature.[30,32] Therefore, heterostructured composites show a slightly lower surface area with respect to pristine TiO_2.

Table 1 Surface, structural and photocatalytic characterization for TiO_2/Er-$BiVO_4$ heterostructured catalysts

Samples	Crystallite size[a] (nm)	BET (m^2 g^{-1})	Band gap (eV)
TiO_2	14 (a)	102	3.14
Er-$BiVO_4$ 0.5%	15 (a)	99	3.14
Er-$BiVO_4$ 1.0%	15 (a)	91	3.13
Er-$BiVO_4$ 2.0%	15 (a)	90	3.13
Er-$BiVO_4$ 3.0%	15 (a)	92	3.07
Er-$BiVO_4$ 4.0%	15 (a)	89	3.05
Er-$BiVO_4$ 5.0%	15 (a)	90	2.80
Er-$BiVO_4$	52 (ts)	3	2.80 + 2.35
$BiVO_4$	48 (ms)	1	2.35

[a] (a: anatase, ts: tetragonal scheelite; ms: monoclinic scheelite).

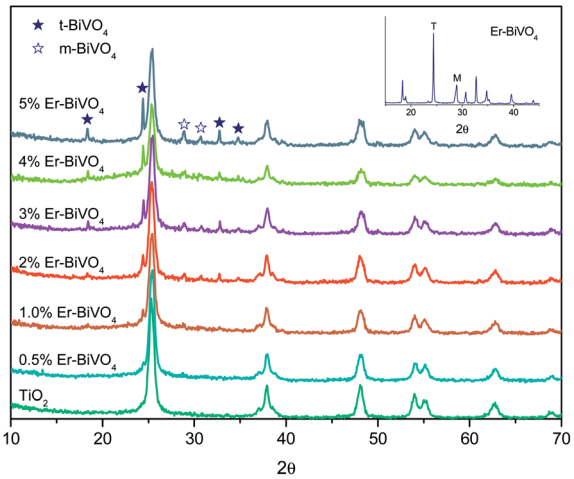

Fig. 1 XRD patterns for TiO_2/Er-$BiVO_4$ heterostructures with different Er-$BiVO_4$ content.

From Raman spectroscopy it is possible to obtain interesting information from the structural point of view (Fig. 2). For bare TiO_2 we have found the typical Raman bands associated to anatase structure: 150 (*e.g.* (1)), 196 (*e.g.* (2)), 396 (A_{1g}/B_{1g}), 516 (A_{1g}), and 640 cm^{-1} (*e.g.* (3)). Single $BiVO_4$ system shows Raman bands around 158, 208, 324, 362, 710, and 826 cm^{-1} were observed for all samples, which are typical vibrational bands of monoclinic $BiVO_4$ (inset in Fig. 2).[43,44] Raman bands at 324 and 366 cm^{-1} are assigned to the asymmetric and symmetric deformation modes of the VO_4^{3-} tetrahedron, respectively.

Additionally, the Raman bands at 822 cm^{-1} corresponds to the symmetric V–O stretching mode with A_g symmetry. When tetragonal phase is present, it can be observed a notably shift of this later band toward higher frequencies (*ca.* 850 cm^{-1}). Thus in our case, in which $BiVO_4$ appears composed by a mixture of tetragonal and monoclinic phase, with the former as the main crystalline phase, only the 850 cm^{-1} is clearly observable.

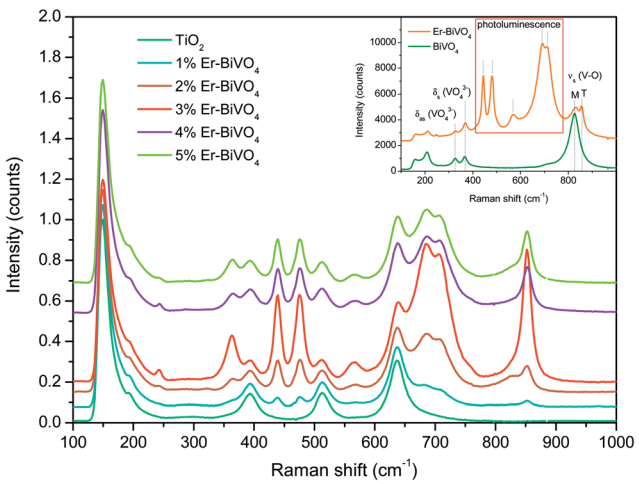

Fig. 2 Raman spectra for TiO_2/Er-$BiVO_4$ heterostructures with different Er-$BiVO_4$ content.

In addition the above structural characterization, it can be stated a set of bands in the range 400–700 nm that could be attributed to the visible fluorescence emission in Er-doped systems (inset in Fig. 2). Such visible luminescence upon green excitation has been widely reported for Er based phosphors materials. As we have previously shown, such emission is related to the presence of tetragonal phase.[30] The Er-doping onto $BiVO_4$ structure is achieved by an effective Er substitution in Bi^{3+} sites of the tetragonal structure. Within this situation, a strong luminescence emission is observed. Therefore, the additional bands observed in the heterostructured composite spectra correspond to such visible luminescence process.

The morphology of $BiVO_4$ has extensively reported to be dependent on the preparation route.[45] In our case, bare $BiVO_4$ shows a square rod-like morphology.[30] The morphology of Er-doped systems clearly denotes the tetragonal-monoclinic structural mixture (Fig. 3a). Thus, both morphologies (square rods and needle-like particles) clearly cohabit in this system. Heterostructured composites are formed by Er-$BiVO_4$ effectively covered by TiO_2 (Fig. 3b and c). Additionally, it can be noticed large TiO_2 aggregates formed by small particles of about 10–15 nm size (inset Fig. 3c and EDS spectra).

Regarding to UV-vis absorption properties, the diffuse reflectance UV-vis spectra of different composites are shown in Fig. 4. As it can be noticed three absorption edges can be found, corresponding to TiO_2 anatase and monoclinic and tetragonal mixture for Er-$BiVO_4$ (inset Fig. 4). The calculated band gap values (Table 1) are in accordance to the heterostructured assembly of TiO_2 and Er-$BiVO_4$ systems. It is worthy to note that due to the low doping level, it is not possible to detect the excitation bands for Er^{3+} species. In spite of this, the strong fluorescence bands observed in Raman spectra would indicate the important luminescence process which is taking place.

The photocatalytic performance of the Er-doped systems was studied for phenol degradation under solar-like irradiation (Fig. 5). The first point that is worthy to mention is that heterostructured composite systems lead to higher photoactivities than bare TiO_2. Thus, as Er-$BiVO_4$ content increases it can be notice a progressive raise in the reaction rates till Er-$BiVO_4$ content reaches 1 wt% value (Fig. 5b). From this value, the

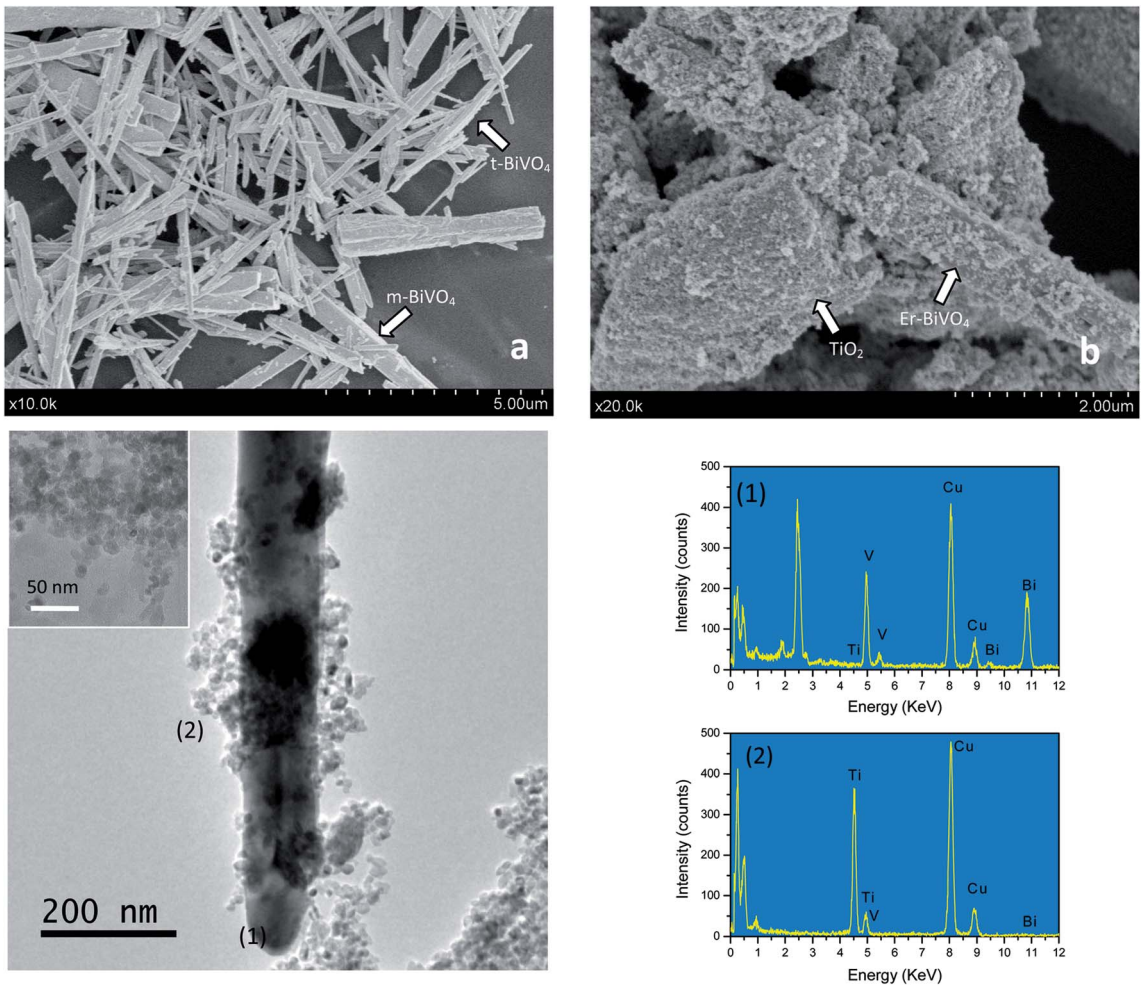

Fig. 3 SEM and TEM study of heterostructured systems: (a) SEM image of Er-$BiVO_4$; (b) SEM image for TiO_2/Er-$BiVO_4$ (1% Er-$BiVO_4$) heterostructures; (c) TEM image for TiO_2/Er-$BiVO_4$ (1% Er-$BiVO_4$) heterostructure including EDS analysis for different positions in the heterostructure interface (inset: TEM image for pristine TiO_2).

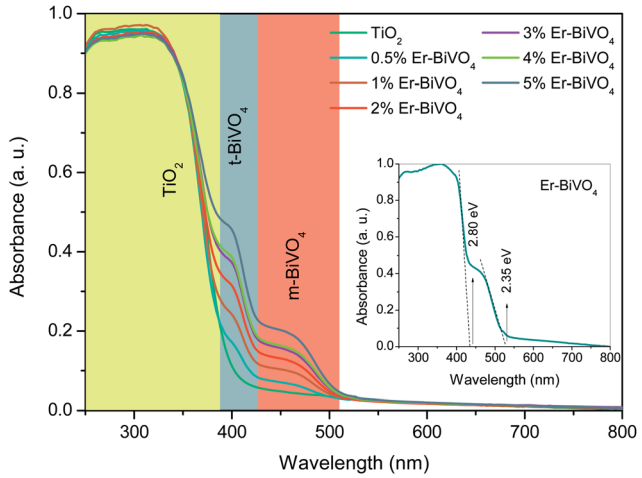

Fig. 4 Diffuse reflectance spectra for TiO_2/Er-$BiVO_4$ heterostructures with different Er-$BiVO_4$ contents.

reaction rate starts to decrease reaching a similar value as pristine TiO_2 for 5 wt%.

The photocatalytic performance of the proposed complex heterostructure clearly overcomes the already published $BiVO_4$–TiO_2 systems.[36,37] Thus, Hu *et al.* proposed a band configuration in which upon visible excitation $BiVO_4$ would act as sensitizer. Based on the position of $BiVO_4$ and TiO_2 conduction bands the photogenerated electron transfer from $BiVO_4$ to TiO_2 is energetically forbidden. So, a different electronic mechanism should be considered in this case. Moreover, Zhang *et al.* showed an interesting synergistic effect taking into account the double UV and visible photoactivity of the $BiVO_4$/TiO_2 heterostructure.[37] However, these authors were able to discolorate Rhodamine B after 6 hours of irradiation. Thus, the results presented here clearly surpass the above mentioned published ones.

In order to envisage a possible mechanism, we have also performed the photoactivity studies for heterostructure composite formed by TiO_2 and undoped *m*-$BiVO_4$ (Fig. 6). Firstly, it is worthy to note that *m*-$BiVO_4$ showed a lower photoactivity than Er-$BiVO_4$ for which a mixture of tetragonal and monoclinic phase is present. This fact was already stated by us and explained by considering a double cooperative photonic and electronic mechanism involved.[30,32]

Regarding to heterostructured composite systems, it is clear that the TiO_2/*m*-$BiVO_4$ assembly, though increases the photoactivity with respect to TiO_2, shows a reaction rate still fairly lower than TiO_2/Er-$BiVO_4$ heterostructure. Taking into account the low Er doping level in the TiO_2/Er-$BiVO_4$ composite (0.75 at.% Er-$BiVO_4$ is present in 1 wt% of the composite), for these heterostructure it would be expected that the up-conversion luminescent process might be almost negligible. So, the enhanced photocatalytic activity must be associated to the presence of an effective intimate heterojunction. Thus, an

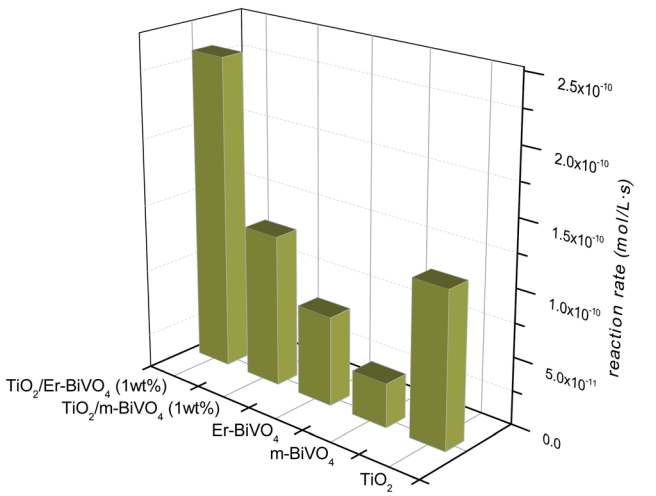

Fig. 6 Comparison of phenol photodegradation reaction rates for different bares and heterostructured materials.

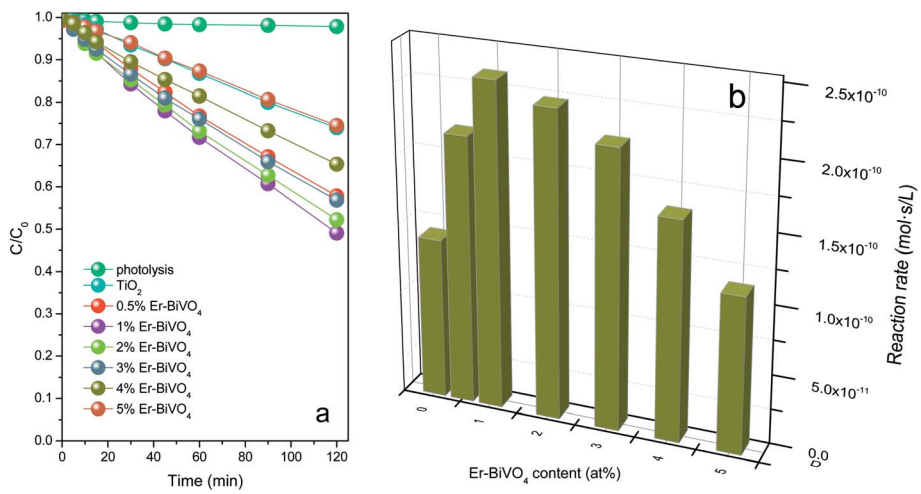

Fig. 5 (a) Evolution of phenol concentration (C_0 = 50 ppm) with photodegradation time; (b) calculated reaction rates for TiO_2/Er-$BiVO_4$ heterostructures with different Er-$BiVO_4$ content.

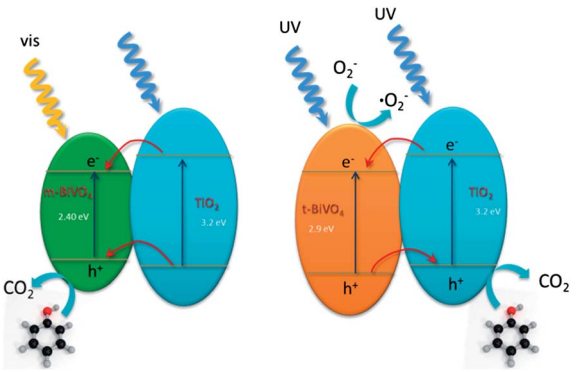

Scheme 2 Proposed electronic mechanism upon UV-vis excitation for different TiO_2–$BiVO_4$ heterostructures.

effective spatial charge separation would be the responsible of the photocatalytic activity enhancement (Scheme 2).

If we consider the band positions for different phases, the difference in the observed band gap values for monoclinic and tetragonal structures lays on the participation of Bi6s orbitals in the monoclinic valence band hybridization.[16] The participation of Bi6s orbital in the band hybridization would stabilize the valence band top through coupling Bi6s–O2p antibonding state with Bi6p state.[2,46] Moreover, the sterically active $Bi6s^2$ lone pair would play a key role in raising up the O2p states and reducing the band gap.[15] From the calculated energies for $BiVO_4$ valence and conduction bands,[47] the following scheme can be envisaged: *m*-$BiVO_4$ valence band top is positioned at slightly lower energy with respect to the TiO_2 one, while the corresponding for *t*-$BiVO_4$ is located at slightly higher energy position (Scheme 2).

On this basis, it could be expected that upon UV excitation, *t*-$BiVO_4$ would act as electron sink while holes will be derived to TiO_2. In the case of TiO_2/*m*-$BiVO_4$ the charge pairs flow in the *m*-$BiVO_4$ direction. For this reason, the reaction rate for TiO_2/*m*-$BiVO_4$ appears comparable than that obtained for TiO_2. Thus, it can be assumed that the occurrence of a structural mixture in the $BiVO_4$ with predominant tetragonal phase would also help to enhanced charge separation. In addition to this proposed synergistic mechanism in a lower extent, the occurrence of a tetragonal-monoclinic heterostructured $BiVO_4$ has been also demonstrated to have better photocatalytic performances.[31] From the relative band positions for tetragonal and monoclinic structures an effective charge separation can be also considered. Therefore, this additional interactive process, though in lower level due to the small $BiVO_4$ content, might be also considered in the overall photocatalytic mechanism.

4. Conclusions

We have obtained a complex heterostructured system by a simple impregnation method, showing improved photoactivity under solar-like irradiation. From this method we have obtained an effective coverage of large Er-$BiVO_4$ particles with 15 nm size TiO_2. From the structural point of view we have stated that the existence of a phase mixture in $BiVO_4$ leads to better photocatalytic performance of the heterojunction. From the results obtained, it would be proposed that the concurrence of TiO_2 and Er^{3+}-$BiVO_4$ complex heterostructure would induce an improved performance due to an optimized charge separation process.

Acknowledgements

The financial support by projects P09-FQM-4570 and ENE2011-24412 is fully acknowledged. S. Obregón thanks CSIC for the concession of a JAE-Pre grant.

References

1 A. Kubacka, M. Fernández-García and G. Colón, *Chem. Rev.*, 2012, **112**, 1555–1614.
2 A. Kudo, K. Omori and H. Kato, *J. Am. Chem. Soc.*, 1999, **121**, 11459–11467.
3 J. Yu and A. Kudo, *Adv. Funct. Mater.*, 2006, **16**, 2163–2169.
4 Y. Sasaki, A. Iwase, H. Kato and A. Kudo, *J. Catal.*, 2008, **259**, 133–137.
5 G. Xi and J. Ye, *Chem. Commun.*, 2001, 1893–1895.
6 S. Navalón, A. Dhkshinamoorthy, M. Alvaro and H. García, *ChemSusChem*, 2013, **6**, 562–577.
7 L. Zhou, W. Z. Wang, L. S. Zhang, H. L. Xu and W. Zhu, *J. Phys. Chem. C*, 2007, **111**, 13659–13664.
8 Y. Zhao, Y. Xie, X. Zhu, S. Yan and S. X. Wang, *Chem. – Eur. J.*, 2008, **14**, 1601–1606.
9 H. Jiang, H. Dai, X. Meng, L. Zhang, J. Deng, Y. Liu and C. T. Au, *J. Environ. Sci.*, 2012, **24**, 449–457.
10 H. Jiang, X. Meng, H. Dai, J. Deng, Y. Liu, L. Zhang, Z. Zhao and R. Zhang, *J. Hazard. Mater.*, 2012, **217–218**, 92–99.
11 A. R. Lim, S. H. Choh and M. S. Jang, *J. Phys.: Condens. Matter*, 1995, **7**, 7309–7324.
12 G. Li, Y. Bai and W. F. Zhang, *Mater. Chem. Phys.*, 2012, **136**, 930–934.
13 J. Yu, Y. Zhang and A. Kudo, *J. Solid State Chem.*, 2009, **182**, 223–228.
14 S. Tokunaga, H. Kato and A. Kudo, *Chem. Mater.*, 2001, **13**, 4624–4628.
15 Z. Zhao, Z. Li and Z. Zou, *Phys. Chem. Chem. Phys.*, 2011, **13**, 4746–4753.
16 Y. Park, K. J. McDonald and K. S. Choi, *Chem. Soc. Rev.*, 2013, **42**, 2321–2337.
17 X. Zhang, Z. Ai, F. Jia, L. Zhang, X. Fan and Z. Zou, *Mater. Chem. Phys.*, 2007, **103**, 162–167.
18 Y. Liu, B. Huang, Y. Dai, X. Zhang, X. Qin, M. Jiang and M.-H. Whangbo, *Catal. Commun.*, 2009, **11**, 210–213.
19 H. M. Zhang, J. B. Liu, H. Wang, W. X. Zhang and H. Yan, *J. Nanopart. Res.*, 2008, **10**, 767–774.
20 S. J. Hong, S. Lee, J. S. Jang and J. S. Lee, *Energy Environ. Sci.*, 2011, **4**, 1781–1787.
21 W. Yao, H. Iwai and J. Ye, *Dalton Trans.*, 2008, 1426–1430.
22 M. Long, W. Cai and H. Kisch, *J. Phys. Chem. C*, 2008, **112**, 548–554.
23 X. Zhang, Y. Gong, X. Dong, X. Zhang, C. Ma and F. Shi, *Mater. Chem. Phys.*, 2012, **136**, 472–476.

24 N. Murakami, N. Takebe, T. Tsubota and T. Ohno, *J. Hazard. Mater.*, 2012, **211–212**, 83–87.
25 D. Wang, R. Li, J. Zhu, J. Shi, J. Han, X. Zong and C. Li, *J. Phys. Chem. C*, 2012, **116**, 5082–5089.
26 W. J. Luo, Z. S. Li, T. Yu and Z. G. Zou, *J. Phys. Chem. C*, 2012, **116**, 5076–5081.
27 K. P. S. Parmar, H. J. Kang, A. Bist, P. Dua, J. S. Jang and J. S. Lee, *ChemSusChem*, 2012, **5**, 1926–1934.
28 G. Tan, L. Zhang, H. Ren, S. Wei, J. Huang and A. Xia, *ACS Appl. Mater. Interfaces*, 2013, **5**, 5186–5193.
29 H. Fan, T. Jiang, H. Li, D. Wang, L. Wang, J. Zhai, D. He, P. Wang and T. Xie, *J. Phys. Chem. C*, 2012, **116**, 2425–2430.
30 S. Obregón, S. W. Lee and G. Colón, *Dalton Trans.*, 2014, **43**, 311–316.
31 S. Usai, S. Obregón, A. I. Becerro and G. Colón, *J. Phys. Chem. C*, 2013, **117**, 24479–24484.
32 S. Obregón and G. Colón, submitted.
33 M. Long, W. Cai, J. Cai, B. Zhou, X. Chai and Y. J. Wu, *J. Phys. Chem. B*, 2006, **110**, 20211–20216.
34 H. Jiang, M. Nagai and K. Kobayashi, *J. Alloys Compd.*, 2009, **479**, 821–827.
35 J. Su, X. X. Zou, G. D. Li, X. Wei, C. Yan, Y. N. Wang, J. Zhao, L. J. Zhou and J. S. Chen, *J. Phys. Chem. C*, 2011, **115**, 8064–8071.
36 Y. Hu, D. Li, Y. Zheng, W. Chen, Y. He, Y. Shao, X. Fu and G. Xiao, *Appl. Catal., B*, 2011, **104**, 30–36.
37 L. Zhang, G. Tann, S. Wei, H. Ren, A. Xia and Y. Luo, *Ceram. Int.*, 2013, **39**, 8597–8604.
38 M. C. Hidalgo, M. Aguilar, M. Maicu, J. A. Navío and G. Colón, *Catal. Today*, 2007, **129**, 50.
39 S. Obregón and G. Colón, *J. Photochem. Photobiol., A*, 2013, **253**, 16.
40 C. T. Au and W. D. Zhang, *J. Chem. Soc., Faraday Trans.*, 1997, **93**, 1195–1204.
41 H. Jiang, H. Dai, X. Meng, K. Ji, L. Zhang and J. Deng, *Appl. Catal., B*, 2011, **105**, 326–334.
42 S. Obregón, A. Caballero and G. Colón, *Appl. Catal., B*, 2012, **117–118**, 59–66.
43 J. Liu, H. Wang, S. Wang and H. Yan, *Mater. Sci. Eng., B*, 2003, **104**, 36–39.
44 J. Yu and A. Kudo, *Chem. Lett.*, 2005, **34**, 850–851.
45 L. Ren, L. Ma, L. Jin, J. B. Wang, M. Qiu and Y. Yu, *Nanotechnology*, 2009, **20**, 405602.
46 K. E. Kweon and G. S. Hwang, *Phys. Rev. B: Condens. Matter*, 2012, **86**, 165209.
47 J. Yang, D. Wang, X. Zhou and C. Li, *Chem. – Eur. J.*, 2013, **19**, 1320–1326.

